water

MDPI

Article

Hygroscopic Water Retention and Physio-Chemical Properties of Three In-House Produced Biochars from Different Feedstock Types: Implications on Substrate Amendment in Green Infrastructure

Xia Bao [1], Manqi Li [1], Renjie Niu [1], Jinling Lu [1], Sagarika Panigrahi [2], Ankit Garg [1,*] and Christian Berretta [3]

[1] Guangdong Engineering Center for Structure Safety and Health Monitoring, Department of Civil and Environmental Engineering, Shantou University, Shantou 515063, China; 20xbao1@stu.edu.cn (X.B.); 18mqli3@stu.edu.cn (M.L.); 18rjniu@stu.edu.cn (R.N.); 19jllu@stu.edu.cn (J.L.)
[2] Department of Civil Engineering, Sree Vidyanikethan Engineering College, Tirupati 517102, India; panigrahisagarika1@gmail.com
[3] School of Civil Engineering, University of Leeds, Leeds LS2 9JT, UK; c.berretta@leeds.ac.uk
* Correspondence: ankit@stu.edu.cn

Abstract: Recent studies have proposed usage of biochar as a substrate amendment in green infrastructure, such as green roofs and bio-filtration units. However, understanding of the variation in physio-chemical properties of biochar due to the production process and feedstock is still lacking. The present study investigated the effects of pyrolysis temperature and feedstocks on the hygroscopic water content and physio-chemical properties of biochar. Biochars were produced from three feedstock types, invasive vegetation (i.e., water hyacinth), non-invasive vegetation (i.e., wood) and one animal waste (i.e., chicken manure). Biochar was produced at two different pyrolysis temperatures (i.e., 300 °C and 600 °C). Scanning electron microscopy + energy dispersive spectrometry (SEM + EDS), Fourier transform infrared spectroscopy (FTIR), X-ray diffraction (XRD), and Brunauer-Emmett-Teller (BET) were performed on all samples to analyze the surface morphology, pore size, element content, functional groups, and chemical bonds. Relative humidity was adjusted to reflect the biochar's hygroscopic property by measuring the maximum moisture content at the sample equilibrium state. The characterization reveals that the lowest carbon content (42.78%) was found at 300 °C for water hyacinth biochar (WHB). The highest carbon content (92.14%) was found at 600 °C for wood biochar (WB). As the pyrolysis temperature increased, the mean pore volume (from 0.03 to 0.18 cm^3/g) and diameter (from 8.40 to 10.33 nm) of the WHB increased. However, the pore diameter of chicken manure (CB) decreased (from 9.23 nm to 7.53 nm) under an increase in pyrolysis temperature. For a given pyrolysis temperature, the hygroscopicity of WHB was highest among all biochars. With an increase in pyrolysis temperature, the hygroscopicity of biochars changed differently. The hygroscopicity of WHB decreased from 82.41% to 44.33% with an increase of pyrolysis temperature. However, the hygroscopicity of CMB and WB remained unchanged. This study suggests that production process of biochars need to be considered for appropriate selection as substrate material in green infrastructure. Further, it promotes the establishment of commercial production of biochar for usage in green infrastructure.

Keywords: biochar; pyrolysis; agricultural waste management; surface characteristic; green infrastructure; soil amendments

Citation: Bao, X.; Li, M.; Niu, R.; Lu, J.; Panigrahi, S.; Garg, A.; Berretta, C. Hygroscopic Water Retention and Physio-Chemical Properties of Three In-House Produced Biochars from Different Feedstock Types: Implications on Substrate Amendment in Green Infrastructure. *Water* **2021**, *13*, 2613. https://doi.org/10.3390/w13192613

Academic Editor: Jiangyong Hu

Received: 15 August 2021
Accepted: 9 September 2021
Published: 23 September 2021

1. Introduction

Biochar, a black high porous material with high carbon content produced by pyrolysis (thermochemical decomposition under a low or no oxygen state) of organic material has been receiving increased attention in the last few decades [1–4]. It has already been widely used for organic solid waste composting, decontamination of water and wastewater, as a catalyst and activator, electrode materials and as an electrode modifier. However, different

studies have investigated the use of biochar as a substrate amendment to optimize the performance of green infrastructure [5]. Several studies have promoted the use of biochar as an amendment in substrate materials in green infrastructure [6–8]. This is mainly due to three factors: firstly, the large specific surface area and porous structure results in enhanced adsorption performance and water retention behavior [9–12]. Secondly, biochar can be used as a conditioner in soil to increase P and K availability in soil, regulate soil pH, thus promoting plant growth and improving crop yield [13,14]. In addition, biochar is also an adsorbent for the removal of heavy metals and phosphate pollutants [15–18]. Thirdly, it is useful for carbon sequestration. The function and application of biochar is mainly governed by its physicochemical properties. For instance, biochar with rich nutrients can be used as soil amendments to improve soil fertility whereas biochar with a highly porous structure can be used as a sorbent [5,19–21]. Biochar that is highly recalcitrance in nature can be used for carbon fixation [19,22–24]. The application of biochar in green infrastructure or for improving soil fertility is an old tradition, commonly used by farmers of China, India, Europe, Japan, and America. In the literature, it has been reported that the amelioration of soil with biochar can improve nutrient retention capacity and ultimately improve soil fertility. It has also been reported that biochar-embedded soil improved the seasonal net primary production. The physicochemical properties of biochar are directly dependent on the preparation procedure (highest treatment temperature, holding time, pyrolysis atmosphere, etc.) and feedstock properties (both physical and chemical) [25,26]. Among the above-mentioned parameters, feedstock property and pyrolysis temperature play a crucial role in the determination of the physicochemical properties of biochar. For example, in the study of Pariyar et al. [27], an increase in pH and BET surface area was noticed, along with an increase in temperature.

Biochar can be prepared by slow pyrolysis, fast pyrolysis, flash carbonization, and gasification [28–30]. Slow pyrolysis is a technique that uses a relatively long residence time (hours to days) and a low heating rate (300 and 700 °C). The peak temperature is the highest temperature reached during the pyrolysis process, which also plays a crucial role in influencing physio-chemical properties [25,26,31]. Generally, the biochar yield decreases as the temperature increases [32–34]. However, the fixed-carbon content in biochar increases by increasing the peak temperature [31,35]. This increase is pronounced in the temperature range from 300 °C to 500 °C. Generally, for most biochar, before 500 °C, hemicellulose and cellulose are decomposed, and volatile components gets converted to gas [36]. When the peak temperatures are higher than 700 °C, biochar generally lacks adsorptive properties [37,38].

Most of the previous studies focused on characterizing biochar produced from agricultural residue/waste or animal waste. However, there are fewer studies that focus on biochar produced from invasive plants. To the best of the authors' knowledge, the comparison of biochar produced from invasive plants and manure has rarely been reported. Due to globalization, invasive plants have become a serious problem. Haphazard growth of invasive plants has adverse effects on the natural environment and ecosystems and causes massive national economic losses [39]. For example, in Nigeria, water hyacinth control was estimated to cost $161 to $639 per hectare [40]. Invasive plant management requires energy and is labor intensive and needs regular removal [39]. Since its introduction about seven decades ago, water hyacinth has infested many water bodies across almost half of China's territory [41]. The water hyacinth is also considered to a plant with one of the fastest reproductive abilities in the world [42]. The use of invasive plants in other applications is a valuable effort. Typically, the water hyacinth is not used after removal and is eventually wasted and will further produce weeds if left; thus, using these invasive plants as a feedstock can provide a better substitute for waste management. Although few studies on the physical and chemical characteristics of biochar produced from invasive weeds have already been published [43–45], limited information is available on the biochar properties derived from a wide range of feedstocks under different pyrolysis temperatures. Hygroscopic water retention is an important characteristic that determines the ability of a

material to absorb moisture from air at a given relative humidity. Such a characteristic can further help to select appropriate biochar as a substrate material in green infrastructure. Based on previous studies, the type of biomass has an effect on the hygroscopicity of biochar [46]. Different pyrolysis temperatures show different hygroscopicities and water retentions. Biochar obtained at a high temperature usually has a higher water absorption than that obtained at a low temperature [47].

The objectives of this study are to compare the hygroscopic water retention and physio-chemical properties of biochar produced from three different feedstocks (invasive vegetation, non-invasive vegetation, and animal waste) and peak temperatures. Previous literature focused on the physical and chemical properties of biochar prepared at random combinations of feedstock type and pyrolysis conditions. The novelty of the present study is that it specifically investigates the hygroscopic properties of biochar produced from three contrasting feedstock types, invasive vegetation (i.e., water hyacinth), non-invasive vegetation (i.e., wood), and an animal waste (i.e., chicken manure).

2. Materials and Methods

2.1. Collection of Biochar Feedstock

Wood and water hyacinth were collected from a local market. The collected materials were initially washed, air dried, and pulverized. Prepared samples were stored in a sealing zip bag for further usage.

2.2. Preparation of Biochar Samples

A programmable muffle furnace (STM-10-13) was used to produce biochar. All raw materials were pyrolyzed at temperatures of 300 °C and 600 °C (heating rate of 10 °C·min^{-1}) for a residence time of 180 min (refer to Table 1), respectively. Biochar was produced under the conditions of filling nitrogen and controlling the temperature, as plotted in Figure 1 and Table 1.

Biochar yield was determined using the following procedure. The weight of the dried pot was recorded as M_1. The dried material was placed into the pot until it was $\frac{3}{4}$ full. The weight of the pot with the dried material was recorded as M_2. Then, the pot was placed into the furnace. The furnace was set as per the designated procedure. After 24 h, the weight of the pot and biochar was measured and noted as M_3. Then, the biochar yield was calculated using the follow equation:

$$\text{Biochar yield (\%)} = (M_3 - M_1)/(M_2 - M_1) \quad (1)$$

The biochar was ground to powder and passed through a 0.9 mm sieve. Then, the biochar was transferred into sealing zip bags and labelled according to their feedstock type. After obtaining biochar, samples were prepared in petri dishes measuring 10.3 cm in diameter and 1.7 cm in height. For ease of interpretation of the results and for comparison, samples were labelled in two parts. The first part was the feedstock of biochar (wood, chicken manure and water hyacinth), and the second part was the pyrolysis temperature (300 °C or 600 °C). For example, Wood 300 represents the sample of wood biochar produced at 300 °C.

Table 1. Temporal setting of pyrolysis process in the thermal decomposition furnace.

Parameter	Value	Remark
c01	0 [a]/0 [b]	The initial temperature of the first stage (°C)
t01	30/60	Operation time of the first stage (min)
c02	300/600	The initial temperature of the second stage (°C)
t02	180/180	Operation time of the second stage (min)
c03	300/600	The initial temperature of the third stage (°C)
t03	30/60	Operation time of the third stage (min)
c04	0/0	The initial temperature of the fourth stage (°C)
t04	−121/−121	Ending order in the program

(Note: [a] and [b] mean the heating routine of low and high pyrolysis processes, respectively).

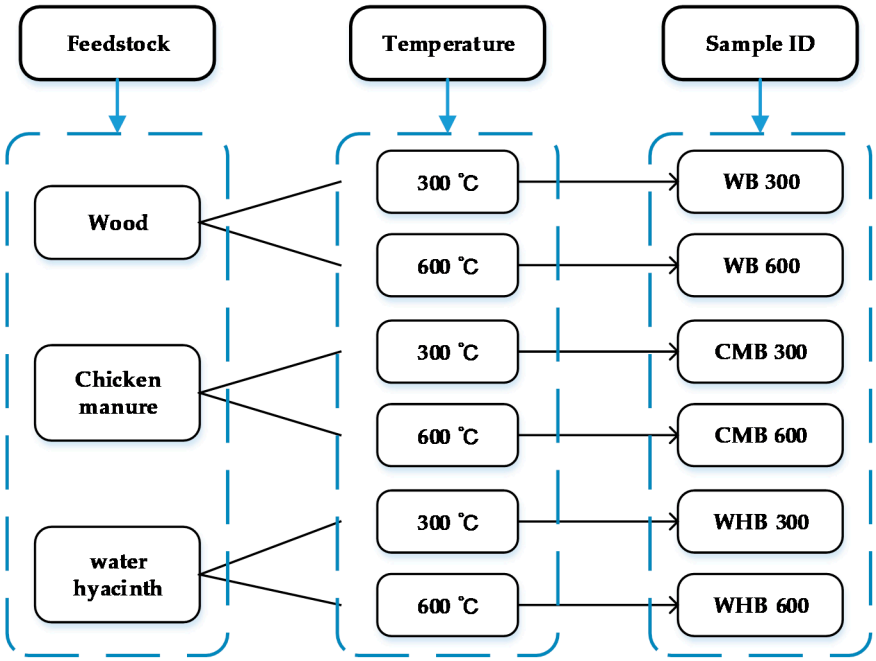

Figure 1. Biochar production conditions and sample grouping.

2.3. Biochar Characterization

2.3.1. Physical and Chemical Structure

The physical structure of biochar prepared from different feedstocks and at varying temperatures was investigated using SEM analysis. Analysis was conducted using Zeiss Supra 40 scanning electron microscopes (Carl Zeiss SMT, Oberkochen, Germany). Simultaneously, the EDX probe mounted to the SEM was used to determine the element content. Appropriate fields were selected for each biochar sample. The element content measured at each target point was averaged. Table 2 summarizes the values of C, O, Na, Mg, Al, Si, P, Cl, K, Ca, S, Rh, B, Te, and Mn for each biochar.

The chemical structure of biochar in the present study was investigated using FTIR (Model: Nicolet is 50, USA) analysis. For this purpose, 1–2 mg of dry biochar was mixed with anhydrous KBr (1:800 by weight) and then ground in an agate bowl and further pressed for infrared scanning. FTIR was used to scan 15 times in the range of a 4000–400 cm^{-1} wave number. The resolution factor was 4 cm^{-1}. The infrared spectrogram was scanned and recorded using a deuterated triglycine sulfate detector.t

Table 2. The average percentages of elements of various biochars at different temperatures.

Element (wt.%)	WB 300	WB 600	CMB 300	CMB 600	WHB 300	WHB 600
C	80.01	92.14	60.15	51.64	42.78	66.35
O	19.43	5.51	20.87	13.54	22.08	10.16
Na	0	0	1.08	2.79	3.43	0.39
Mg	0.11	0.07	0.77	0.30	3.97	0.67
Al	0.05	0.04	0.33	0.00	0.04	0.00
Si	0.00	0.07	0.71	1.33	0.15	0.14
P	0.00	0.02	4.44	1.67	2.65	1.07
Cl	0.00	0.00	0.59	11.27	7.87	6.09
K	0.00	0.56	4.85	15.21	3.82	6.22
Ca	0.45	1.58	5.39	1.65	6.28	8.29
S	0.00	0.00	0.53	0.52	0.09	0.14
Rh	0.00	0.00	0.00	0.00	0.33	0.13
B	0.00	0.00	0.00	0.00	3.44	0.00
Te	0.00	0.00	0.00	0.00	0.31	0.00
Mn	0.00	0.00	0.00	0.00	0.00	0.37
Total	100.05	99.99	99.71	99.92	97.24	100.02

2.3.2. Quantitative Phase Analysis (XRD)

A X-ray diffractometer (D8 ADVANCE) was used to analyze crystallographic structure (atomic and molecular) of biochar. The X-ray diffractometer was operated at 40 kV and 20 mA. The data were collected over a 2θ range of 0–50° using Cu-Kα radiation at a scan rate of 2° min^{-1}. The phase peaks were identified by comparing the observed XRD patterns to the standards compiled by the Joint Committee on Powder Diffraction and Standards (PDF22004).

2.3.3. Brunner Emmet Teller (BET)

The surface area of the biochar was evaluated using the BET method. This method helps to establish adsorption and desorption curves of nitrogen at liquid nitrogen temperatures. Liquid nitrogen volume was obtained by equivalent substitution of capillary condensation and volume, i.e., pore volume and pore diameter distribution. The absorption and desorption curves were transformed into a pore diameter distribution using the BET model method. Based on the principle of equivalent substitution of capillary condensation and volume, liquid nitrogen volume was converted to pore volume. The difference in the characterization structure of the biochar was found through comparative analysis of pore volume and pore size distribution.

2.3.4. Hygroscopicity of Biochar at Different Feedstock and Pyrolysis Temperatures

The hygroscopicity of biochar was investigated by controlling the temperature (30 °C) and changing the relative humidity (RH) [48,49]. The study was conducted for 7 weeks by fixing the humidity chamber temperature to 30 °C. RH was initially set at 90% to allow the sample to absorb enough moisture. Then, RH was adjusted to 50%. At this humidity, the test chamber was relatively dry, and the sample was in a desorption state. When the sample was in the equilibrium stage, the RH was adjusted to 90% with a step interval of 10% RH. Therefore, the experiment was divided into 6 periods according to different RH conditions. The water content of the sample was calculated by continuously recording the change in the sample quality. When it reached equilibrium, the moisture content of each sample was recorded as the maximum moisture content under RH conditions. For better comprehension, the objectives and methodology used in this study are graphically presented in Figure 2.

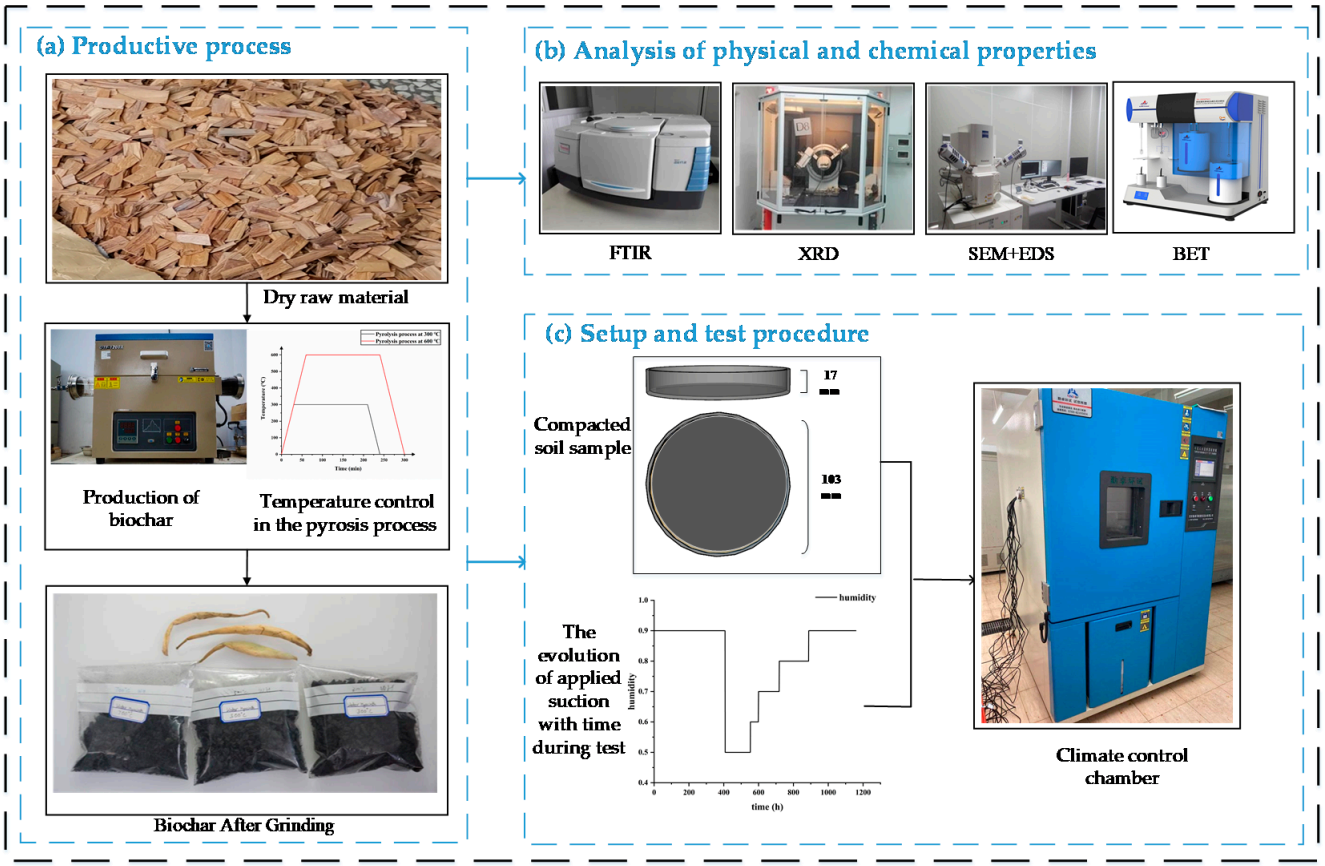

Figure 2. Schematic representation of the objectives of this study.

3. Results

3.1. SEM + EDS

The microstructure of biochar is essential for the water-holding and adsorption capacity of soil [50]. SEM images of biochar prepared from different materials at different temperatures were captured under the same magnification for comparison. At the same pyrolysis temperature, the surface structure of biochar produced from different biomass was significantly different. At 300 °C, the biochar produced from wood was mainly a sheet structure (a), the biochar produced from water hyacinth was mainly a block structure (c), and the biochar produced by chicken manure was mainly a granular structure (e). Biochar produced from plant waste seemed to be more porous than that of chicken manure (i.e., animal waste). In addition, the surface structures of the biochar varied with different pyrolysis temperatures. As observed in the samples produced at 300 °C, they presented smooth and compact surfaces (Figure 3a,c,e). However, the samples pyrolyzed at 600 °C exhibited more porous, rough, or pitted surface textures (Figure 3b,d,f) indicating more amount of charring of the material at a higher pyrolysis temperature. Such micro-structures can have implications on water retention performance in green infrastructure. Biochar produced from plant waste may tend to absorb more water than that of animal waste. The hygroscopicity of plant-based biochar is strong. Biochar produced from plant appears to have a larger specific surface area than that produced from chicken manure. Mangrich et al. showed that a high surface area of the biochar can improve the water holding capacity of soil [49,51–53]. However, from a SEM image, it may not be conclusive to how pyrolysis temperature would influence water retention.

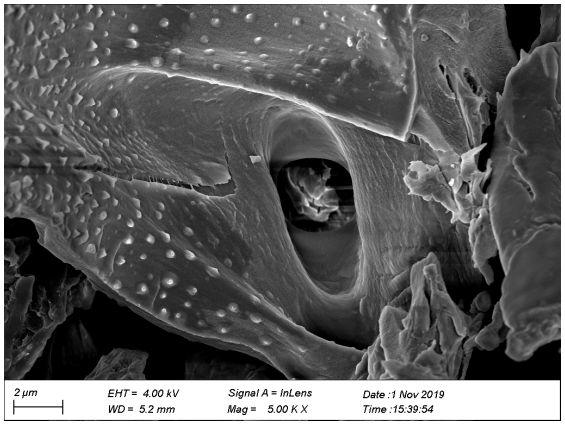

(**a**) Biochar made from wood at 300 °C

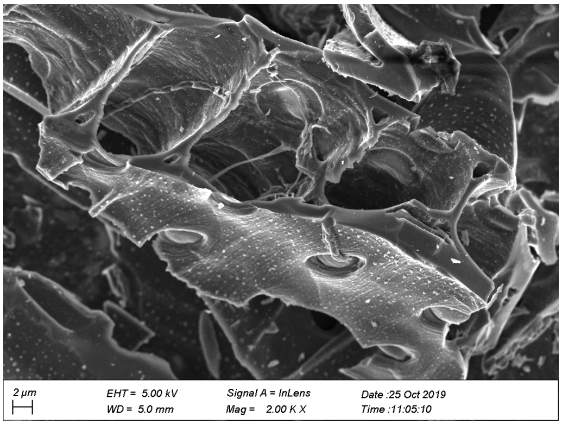

(**b**) Biochar made from wood at 600 °C

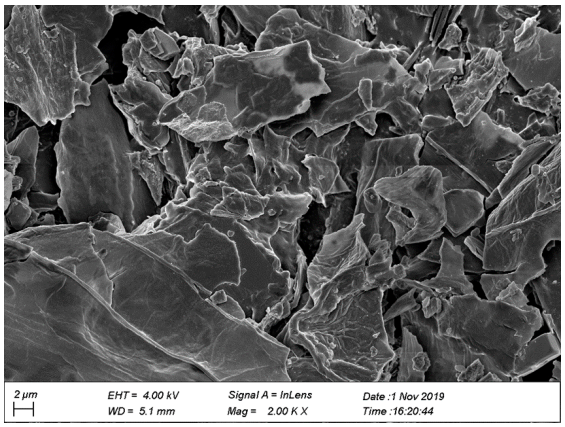

(**c**) Biochar made from water hyacinth at 300 °C

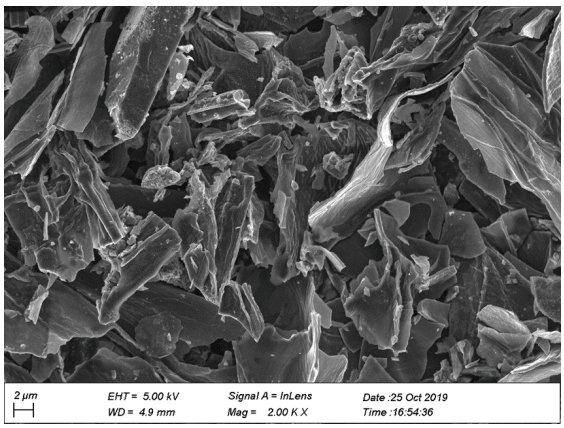

(**d**) Biochar made from water hyacinth at 600 °C

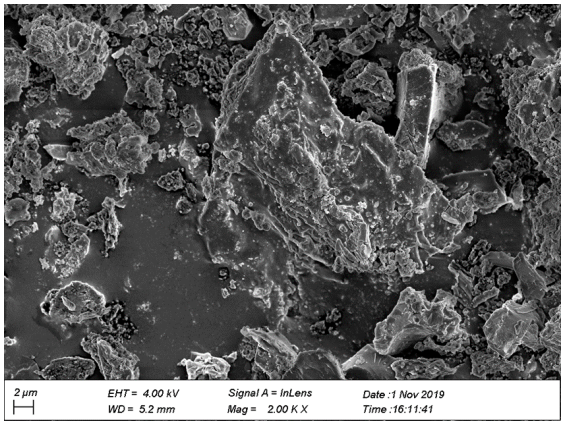

(**e**) Biochar made from chicken manure at 300 °C

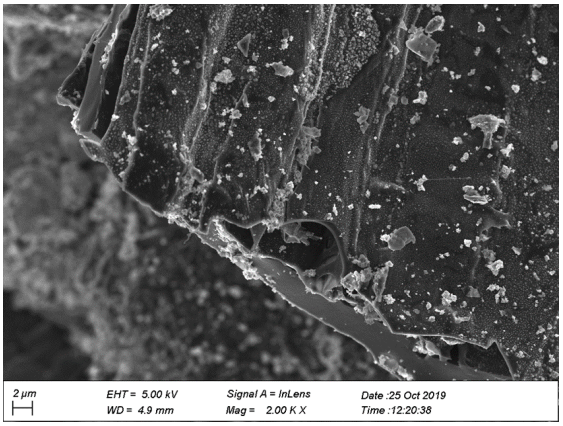

(**f**) Biochar made from chicken manure at 600 °C

Figure 3. The same resolution SEM images of different materials that was pyrolyzed at 300 °C (**a**,**c**,**e**) and 600 °C (**b**,**d**,**f**). Comparing the SEM images of various biochars at different preparation temperatures, the porous structure of biochar gradually becomes obvious and tends to be broken with the increase of pyrolysis temperature.

Table 2 summarizes the relative content of elements of biochar produced by wood, chicken manure, and water hyacinth (at different pyrolysis temperatures). The content of carbon (C) and oxygen (O) of water hyacinth at different pyrolysis temperatures showed an obvious difference. The C and O content for CMB and WB had similar values. As for

water hyacinth, the content of carbon (C) increased from 42.78% to 66.35% upon an increase in pyrolysis temperature from 300 °C to 600 °C. This indicates a higher extent of charring with pyrolysis temperature. On the other hand, the proportion of oxygen (O) reduces from 22.08% to 10.16% with an increase in temperature from 300 °C to 600 °C. A previous study reported that, as the pyrolysis temperature increases, impure volatile products and unstable structures (oxygen (O) and chlorine (Cl)) are gradually reduced, along with the conversion of alkyl and O-alkyl C to aryl C [54].

It can be seen from Table 2 that the proportions of C of CMB (60.15%) and WB (80.01%) were clearly different. The reason for this phenomenon is that the compounds in WB and CMB are disparate. WB is mainly composed of aromatic hydrocarbons and phenols. The aromatic structural components and the alkyl or oxygen-containing heteroatomic groups attached to the aromatic structure constitute biochar [55]. However, the components of CMB are primarily N-heterocyclics and phenols [56]. In addition, the proportion of O in CMB (20.87%) was similar to WB (19.43%).

3.2. FTIR

The effect of feedstock type and pyrolysis temperature on chemical structure of biochar was investigated using FTIR analysis. Figure 4a,b show the spectrums of each biochar at 300 °C and 600 °C, respectively. The overall shapes of this spectrum were very similar for all biochars. Both spectra indicate complex bands at 1800–500 cm^{-1} due to the aromatic C=C band and different substitution reaction of the aromatic ring [57]. The number of characteristic peaks of biochar at 300 °C are greater than at 600 °C. The higher the temperature, more is the decomposition of biochar components. At 600 °C, some functional groups tend to disappear (i.e., characteristic peak as per corresponding wavenumber; [58]). More functionalities can be detected at 300 °C. At 300 °C, some components of cellulose, hemicellulose, and lignin are still retained in biochar, while at 600 °C, the pyrolysis components are mainly aromatic compounds with reduced oxygen and increased carbon [59].

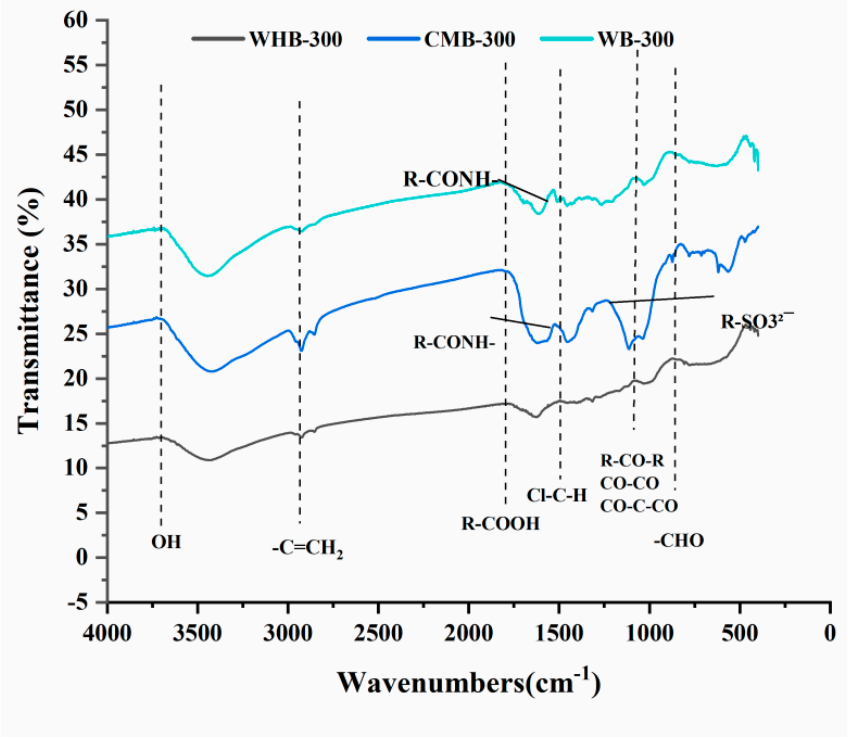

(a)

Figure 4. *Cont.*

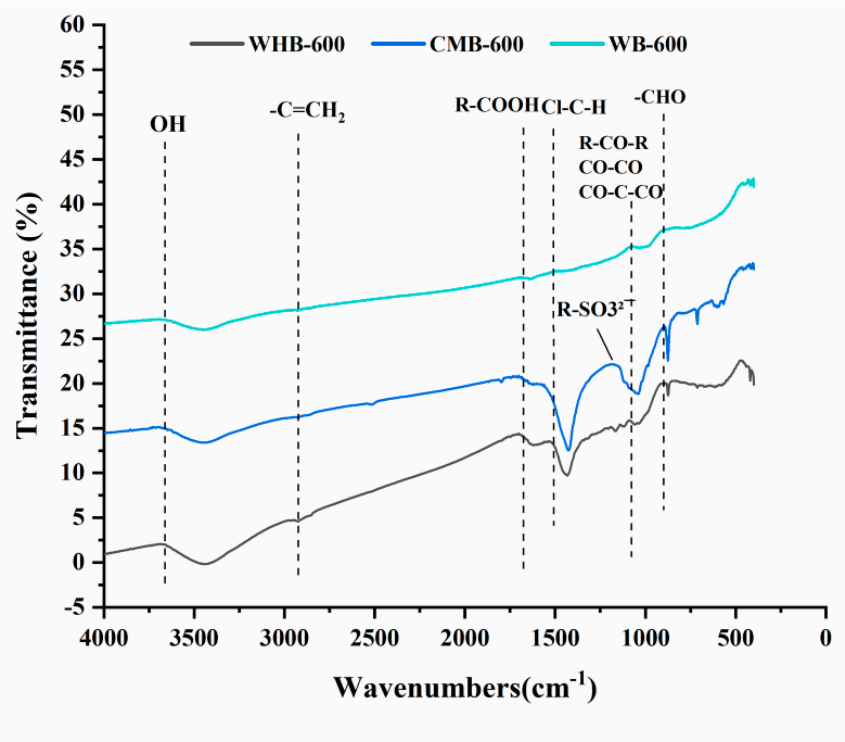

(**b**)

Figure 4. (**a**) FTIR spectrum of biochar prepared at 300 °C. (**b**) FTIR spectrum of biochar prepared at 600 °C.

Table 3 summarizes the functional groups of all types of biochar. Both spectra show an obvious band at 3700 and 3200 cm^{-1} due to the stretching vibration of –OH of the alcohol and phenol associated with intermolecular hydrogen bonding. With an increase in pyrolysis temperature, –OH is continuously lost. They also show bands at 3200–2920 cm^{-1} corresponding to the stretching vibration of $–CH_3$. The pyrolyzed WB and CMB obtained at 600 °C do not contain $–CH_3$. This indicates that $–CH_3$ has been decomposed during the heating process from 300 °C to 600 °C. The bands at 1820 cm^{-1}–1670 cm^{-1} were due to the stretching vibration of –COOH. However, WB at 600 °C does not contain these functionalities, indicating that –COOH is also decomposed with an increase in pyrolysis temperature. The bands at 1080–1220 cm^{-1} corresponded to C–O extension. The surface functional groups of biochar from different feedstocks were roughly the same. At higher temperatures, hemicellulose and cellulose tend to decompose more. Reduction in functionalities indicates that biochar produced at higher pyrolysis temperature may have lower tendency to mitigate nutrient leaching, as well as pollutant sorption. This may not be favorable for amendment of a substrate in green infrastructure, which is subjected to higher loads of pollutants in incoming storm water. However, a higher temperature usually leads to more porosity but a reduction in functionalities (essential for pollutant sorption) and can also have a negative impact on the performance of green infrastructure. Future studies are needed to evaluate the effectiveness of biochar (in this study) on water retention and pollutant sorption phenomena in the field.

Table 3. Characteristics wavenumber and the corresponding transmittance of biochar.

Functional Group	WB 300 (%)	WB 600 (%)	CMB 300 (%)	CMB 600 (%)	WHB 300 (%)	WHB 600 (%)
O–H	✔ 3743.154	✔ 3451.955	✔ 3727.726	✔ 3727.726	✔ 3727.726	✔ 3687.228
–C=CH_2	✔ 2985.266		✔ 2996.837		✔ 2985.266	✔ 2948.626
R–COOH	✔ 1824.329		✔ 1820.043	✔ 1700.908	✔ 1793.474	✔ 1700.908
Cl–C–H					✔ 1494.562	
R–CONH-	✔ 1535.059		✔ 1521.56			✔ 1535.059
R–SO_3^{2-}			✔ 1234.219	✔ 1186.007		
R–CO–R CO–CO CO–C–CO	✔ 1072.227	✔ 1072.227			✔ 1083.798	✔ 1087.655
–CHO	✔ 885.166	✔ 879.381			✔ 869.738	✔ 848.525

3.3. BET

Table 4 summarizes the Brunauer-Emmett-Teller (BET) properties (i.e., surface area, pore volume and distribution) of biochar. The specific surface area of biochar is generally larger than that of sandy soil and clay (ref). This suggests that biochar addition to soil can increases its total specific surface area and water storage capacity. The pore structures of biochar produced from different materials at various temperatures are quite different. According to the size of biochar pores, the pores in biochar can be divided into micropores (<0.8 nm), small pores (0.82 nm), medium pores (>2–50 nm), and large pores (>50 nm). Micropores have the greatest effect on the specific surface area of biochar. Micropores are conducive to adsorbing more molecules, such as gases and common solvents. Macropores mainly affect soil permeability and water transport [60]. The specific surface area of micropores in biochar are significantly larger than those of macropores, but the macropores have a larger volume, which will play a more significant role in soil improvement [61]. In the present study, the pores of biochar were mostly mesoporous.

Table 4. Texture properties of materials.

Sample	Surface Area (m^2/g)	The Pore Volume (cm^3/g)	Pore Size Distribution (nm)
WB300	19.81	0.03	6.15
WB 600	73.12	0.15	10.88
CMB 300	19.31	0.05	16.03
CMB 600	75.33	0.15	10.88
WHB 300	15.40	0.03	8.69
WHB 600	62.93	0.20	13.81

3.4. XRD

Figure 5a,b shows the X-ray diffraction for different types of biochar. Biochar phase analysis results made from various materials were compared at 300 °C and 600 °C, respectively. As shown in the figure, the results showed significant differences in the components of biochar of the same species at different pyrolysis temperatures. The biochar prepared at 300 °C was mainly acidic. Cellulose and hemicellulose will decompose at 300 °C, producing organic acids and phenolic substances, reducing the pH value of biological carbon [62]. The biochar prepared at 600 °C was mainly alkaline because the decomposition of organic matter at 600 °C increases the pH value of biochar [63]. Such a change in pH value will have

implications on plant growth and survival in green infrastructure [64]. Highly alkaline biochar may hinder plant growth and also affect pollutant sorption in green infrastructure. The main components of biochar were different at the two temperatures. This indicates that, with an increase in temperature, the composition of biochar will change significantly.

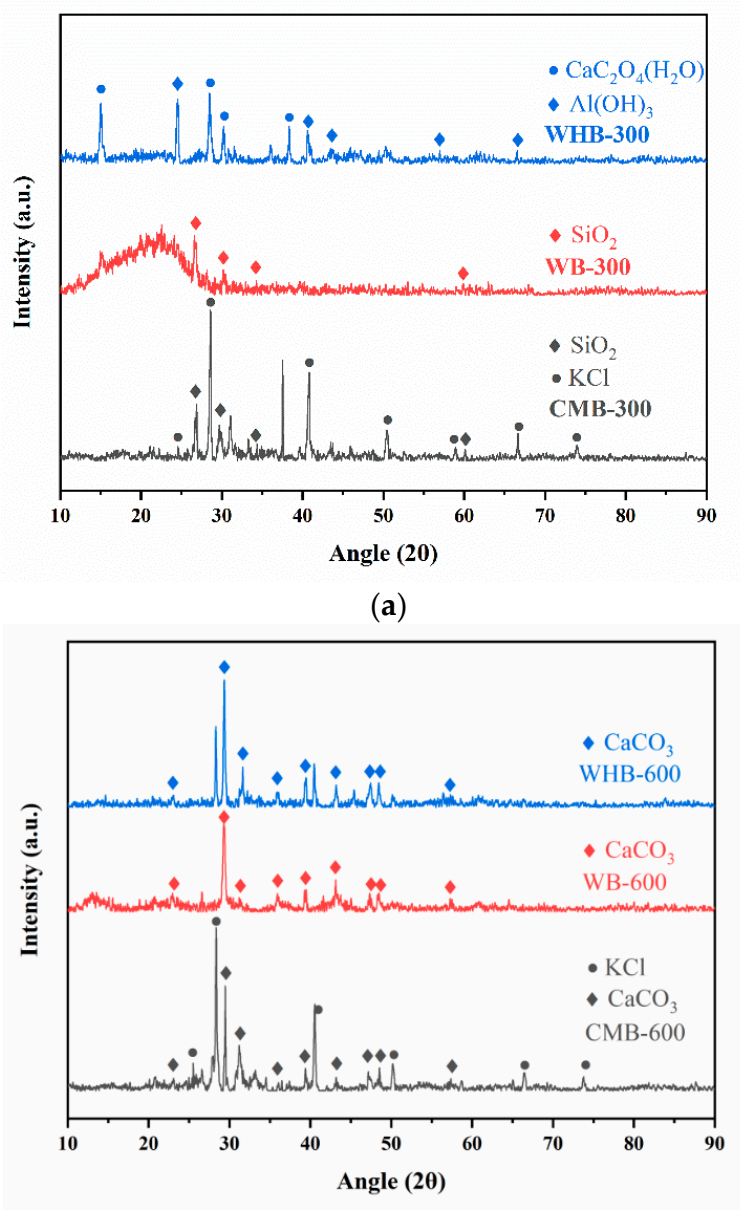

Figure 5. (**a**) XRD results for all biochar samples at 300 °C. (**b**) XRD results for all biochar samples at 600 °C.

At the same pyrolysis temperature, the phase analysis results of different biochars were compared (refer to Figure 5a,b and Table 5). At 600 °C, all biochars contained $CaCO_3$ and CO_3^{2-}, which may play an essential role in adsorption capacity and the removal mechanism of adsorbates [65]. There were significant differences in the composition of all types of biochar at 300 °C. For example, only WB and CMB contained SiO_2. The pyrolysis of biochar was incomplete at 300 °C, as indicated by the XRD pattern. When the temperature increased to 600 °C, the internal components of biochar decomposed. The carbon content was increased with the decrease of oxygen and other elements.

Table 5. Phase analysis results for all biochars.

Sample	Similar Material	Main Ingredients
WHB 300	Aluminum hydroxide	$Al(OH)_3$
WB 300	Quartz	SiO_2
CMB 300	Dolomite, quartz	$Ca_3Mg(CO_3)_2$, SiO_2
WHB 600	Calcite	$CaCO_3$
WB 600	Calcite	$CaCO_3$
CMB 600	Calcium aluminate, calcite	$Ca_3Al_2O_6$, $CaCO_3$

3.5. The Hygroscopicity of Biochar

Figure 6 shows the hygroscopic characteristics of all biochar prepared at 300 °C and 600 °C. The value of the maximum moisture content varied from 5% to 80% for all biochar samples. Among different biochar types at a given pyrolysis temperature (at 300 °C and 600 °C, respectively), it could be concluded that WHB had the strongest hygroscopicity ability, followed by chicken manure biochar. WB had the weakest hygroscopicity ability. This was because, at the same pyrolysis temperature, the hygroscopicity of biochar was mainly affected by the carbon and oxygen content of biochar (i.e., the content of oxygen-containing functional groups; [66]). According to Table 2, it can be observed that the total carbon and oxygen contents of WHB, CMB, and WB were 64.86%, 81.02%, and 99.44% at 300 °C, respectively. The three kinds of biochar's carbon and oxygen content was as follows: WHB < CMB < WB. Therefore, these three kinds of biochar hygroscopicities were manifested as: WHB > CMB > WB.

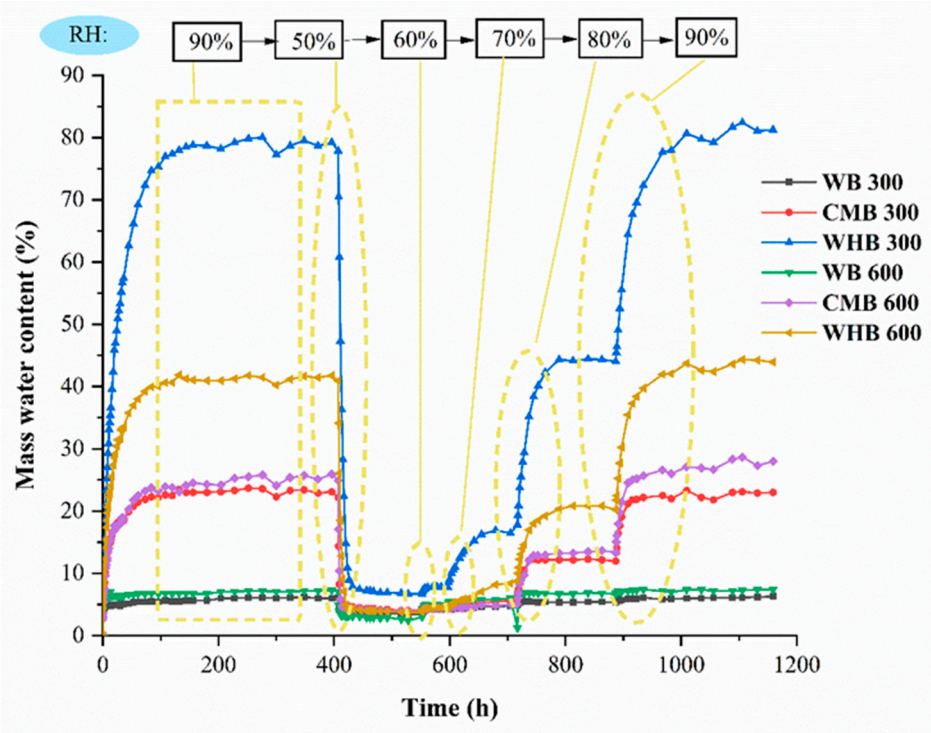

Figure 6. Water absorption behavior of different biochars with time at different relative humidity conditions under 30 °C temperature conditions.

For a given biochar at different pyrolysis temperatures, it could be concluded that the hygroscopicity of WHB prepared at 300 °C was stronger than that prepared at 600 °C. However, the hygroscopicity of CMB and WB did not change significantly with the change in pyrolysis temperature. A possible reason for this phenomenon is that biochar prepared at 300 °C contains hydrophilic oxygen-containing functional groups. These groups tend to decompose at higher pyrolysis temperatures [67,68]. On the other hand, specific surface area and pore volume of biochar are usually enhanced at higher pyrolysis

temperatures [69,70]. The lower hygroscopic nature of WHB-600 as compared to WHB-300 could be due to the fact that the loss of chemical adsorption capacity (due to functional groups) was greater than the enhancement of physical adsorption capacity (due to specific surface area). In the case of CMB and WB, the loss of the chemical adsorption capacity of the functional groups is likely similar to the enhancement of the physical adsorption capacity. It could be seen from Figure 6 that, for each biochar sample, the moisture content of the sample was only related to the temperature and relative humidity of the environment. After changing the humidity, the maximum moisture content of the biochar changed, but eventually it tended to be a stable value.

Table 6 summarizes studies of other scholars on the hygroscopicity of biochar. It can be seen from the table that the feedstocks and pyrolysis temperature have significant influence on the hygroscopicity of biochar [46,48,71]. Compared with other studies, the WHB-300 shows excellent hygroscopicity (maximum moisture content is 79.09%). The hygroscopicity of different biochar in different temperature is quite different. The structure of biochar is affected by pyrolysis temperatures, which affects the water absorption performance of biochar [72]. Therefore, reasonable selection of feedstock and temperature is of great significance to improve the hygroscopicity of biochar in green infrastructure.

Table 6. The performance of biochar on hygroscopicity.

Study	Feedstocks	Pyrolysis Temperature	The Maximum Water Content (%)	Remarks
Gray et al. [71]	hazelnut shells	370 °C	50.62	Hygroscopicity increases with increasing temperature
		620 °C	60.56	
	Douglas fir chips	370 °C	66.18	
		620 °C	73.32	
Chen et al. [48]	Tobacco stem	250 °C	16.38	Hygroscopicity decrease with increasing temperature
		850 °C	12.53	
Jiang et al. [46]	Cedar wood	200 °C	15.72	Hygroscopicity decrease with increasing temperature
		225 °C	14.58	
		250 °C	13.03	
		275 °C	10.20	
		300 °C	7.79	
	Polar wood	200 °C	11.15	
		225 °C	9.64	
		250 °C	8.33	
		275 °C	7.53	
		300 °C	7.37	
	Corn stalk	200 °C	13.74	
		225 °C	12.27	
		250 °C	11.93	
		275 °C	11.47	
		300 °C	11.26	
	Wheat straw	200 °C	17.29	
		225 °C	15.97	
		250 °C	13.97	
		275 °C	12.38	
		300 °C	12.18	
Present study	Water hyacinth	300 °C	79.07	The hygroscopicity of water hyacinth decrease with increasing temperature
		600 °C	41.29	
	Wood	300 °C	6.82	
		600 °C	7.36	
	Chicken manure	300 °C	23.07	
		600 °C	24.61	

Green infrastructure has been extensively advocated to realize sustainable cities and manage storm water. It has been defined as "the network of green spaces and water systems that delivers multiple environmental, social, and economic values and services to urban

communities" [73]. Water holding capacity is considered an important characteristic of green infrastructure and has been studied by many researchers and practitioners in recent years. Some media commonly used for green infrastructure are summarized in Table 7, where it can be noted that most materials can improve the water retention capacity of green infrastructure by 30% to 40% [74–76]; however, water hyacinth biochar produced at 300 °C in this study can significantly improve water retention capacity by about 80%. Furthermore, compared with other materials, biochar has a wider source and lower preparation cost. Therefore, biochar is a promising substrate material in green infrastructure.

Table 7. Summary of media commonly used for green infrastructure.

Study	Materials	Water Holding Capacity (%)
Nagase, A. [74]	Cocopeat	39
	Commercial green roof substrate	37.5
Bollman, M. A. et al. [75]	Peat moss	82.4
	Perlite	57.9
	Pumice	52.5
	Red cinder	20.1
	River sand	44.1
	Vermiculite	41.6
Graceson et al. [76]	Crushed brick	28.2
	Crushed tile	32.5
	Lytag	30.0
Present study	Water hyacinth biochar (300 °C)	79.07
	Water hyacinth biochar (600 °C)	41.29
	Wood biochar (300 °C)	6.82
	Wood biochar (600 °C)	7.36
	Chicken manure (300 °C)	23.07
	Chicken manure (600 °C)	24.60

Such observation has implications while selecting suitable amendment material for substrate in green infrastructure. For areas or regions characterized by higher total rainfall or high humidity, it may be more relevant to use biochar produced from water hyacinth at 300 °C as compared to other types of biochar as listed in Table 7. In addition, the availability of feedstock in that particular region need to be considered for maintaining low cost of production of biochar. Further, a proper cost benefit analysis is also required considering cost of biochar production, as well as long term impact of biochar on green roofs performance and carbon sequestration.

4. Conclusions

In this study, the hygroscopic water retention and physio-chemical properties of biochar prepared using three different raw materials, i.e., invasive vegetation, non-invasive vegetation, and animal waste, at 300 °C and 600 °C, were compared and analyzed. The study shows that the feedstocks and the pyrolysis conditions greatly influence hygroscopic water content and physio-chemical properties of biochar. The surface structure of biochar produced from different feedstock type was significantly different. With an increase of pyrolysis temperature, the aromatization degree of biochar increased, and biochar's stability was greatly improved. Meanwhile, the porous structure of biochar was eventually obvious and tended to be fragmented.

The porosity of biochar and the hydrophilic groups can affect its hygroscopicity. Higher pyrolysis temperature leads to loss of chemical adsorption capacity and the enhancement of physical adsorption capacity. At the same temperature, WHB had the strongest hygroscopicity ability, while wood had the weakest ability of hygroscopicity. Compared with WB, WHB is considered a preferable substrate material in green infrastructure. Except for the WHB, the hygroscopicity of biochar did not change significantly with the change of pyrolysis temperature. The appropriate biochar pyrolysis mode and

feedstocks can be chosen to improve the water retention of substrate in green infrastructure. For minimizing the environmental impact and supporting the implementation of green infrastructure more comprehensive research on the use of produced biochar as soil amendment under extreme climatic conditions (such as drought and freeze–thaw) is encouraged. This study promotes the development of commercial industries that produces specific types of biochar for usage in green infrastructure.

Author Contributions: Conceptualization, X.B., M.L. and A.G.; methodology, R.N.; software, J.L., R.N., J.L. and M.L.; validation, X.B., C.B. and A.G.; formal analysis, J.L., M.L. and A.G.; investigation, X.B., S.P. and A.G.; resources, X.B., M.L. and A.G.; data curation, R.N.; writing—original draft preparation, X.B.; writing—review and editing, R.N. and S.P.; visualization, X.B. and M.L.; supervision, X.B.; project administration, X.B.; funding acquisition, A.G. All authors have read and agreed to the published version of the manuscript.

Funding: The research was funded by the National Natural Science Foundation of China, grant number 41907252.

Institutional Review Board Statement: Not applicable.

Informed Consent Statement: Not applicable.

Data Availability Statement: Some or all data, models, or code that support the findings of this study are available from the corresponding author upon reasonable request.

Conflicts of Interest: The authors declare no conflict of interest.

References

1. Lehmann, J.; Joseph, S. Biochar for environmental management: Science, technology and implementation. *Sci. Technol.* **2015**, *25*, 15801–15811.
2. Downie, A.; Crosky, A.; Munroe, P. Physical properties of biochar. In *Biochar for Environmental Management*; Routledge: London, UK, 2012; pp. 45–64.
3. Liu, W.-J.; Jiang, H.; Yu, H.-Q. Development of Biochar-Based Functional Materials: Toward a Sustainable Platform Carbon Material. *Chem. Rev.* **2015**, *115*, 12251–12285. [CrossRef] [PubMed]
4. Kookana, R.S. The role of biochar in modifying the environmental fate, bioavailability, and efficacy of pesticides in soils: A review. *Soil Res.* **2010**, *48*, 627–637. [CrossRef]
5. Wang, J.; Wang, S. Preparation, modification and environmental application of biochar: A review. *J. Clean. Prod.* **2019**, *227*, 1002–1022. [CrossRef]
6. Wang, Y.; Kang, J.; Jiang, S.; Li, H.; Ren, Z.; Xu, Q.; Jiang, Q.; Liu, W.; Li, R.; Zhang, Y. A composite of Ni–Fe–Zn layered double hydroxides/biochar for atrazine removal from aqueous solution. *Biochar* **2020**, *2*, 455–464. [CrossRef]
7. Wang, H.; Zhang, K.; Gan, L.; Liu, J.; Mei, G. Expansive soil-biochar-root-water-bacteria interaction: Investigation on crack development, water management and plant growth in green infrastructure. *Int. J. Damage Mech.* **2021**, *30*, 595–617. [CrossRef]
8. Huang, S.; Huang, D.; Garg, A.; Jiang, M.; Mei, G.; Pekkat, S. Stormwater management of biochar-amended green roofs: Peak flow and hydraulic parameters using combined experimental and numerical investigation. *Biomass Convers. Biorefinery* **2020**, 1–12. [CrossRef]
9. Zhang, M.; Gao, B.; Yao, Y.; Inyang, M. Phosphate removal ability of biochar/MgAl-LDH ultra-fine composites prepared by liquid-phase deposition. *Chemosphere* **2013**, *92*, 1042–1047. [CrossRef]
10. Ni, J.; Chen, X.W.; Ng, C.W.W.; Guo, H.W. Effects of biochar on water retention and matric suction of vegetated soil. *Géotecnique Lett.* **2018**, *8*, 124–129. [CrossRef]
11. Lim, T.; Spokas, K.; Feyereisen, G.; Novak, J. Predicting the impact of biochar additions on soil hydraulic properties. *Chemosphere* **2016**, *142*, 136–144. [CrossRef] [PubMed]
12. Razzaghi, F.; Obour, P.B.; Arthur, E. Does biochar improve soil water retention? A systematic review and meta-analysis. *Goderma* **2020**, *361*, 114055. [CrossRef]
13. Purakayastha, T.; Bera, T.; Bhaduri, D.; Sarkar, B.; Mandal, S.; Wade, P.; Kumari, S.; Biswas, S.; Menon, M.; Pathak, H.; et al. A review on biochar modulated soil condition improvements and nutrient dynamics concerning crop yields: Pathways to climate change mitigation and global food security. *Chemosphere* **2019**, *227*, 345–365. [CrossRef] [PubMed]
14. Matos, T.T.; Fornari, M.R.; Mangrich, A.S.; Schultz, J.; Batista, E.M.C.; Ribeiro, R.O.; Romão, L.P.; Yamamoto, C.I.; Grasel, F.S.; Bayer, C.; et al. Low temperature production of biochars from different biomasses: Effect of static and rotary lab reactors and application as soil conditioners. *J. Environ. Chem. Eng.* **2021**, *9*, 105472. [CrossRef]
15. Inyang, M.; Gao, B.; Yao, Y.; Xue, Y.; Zimmerman, A.; Pullammanappallil, P.; Cao, X. Removal of heavy metals from aqueous solution by biochars derived from anaerobically digested biomass. *Bioresour. Technol.* **2012**, *110*, 50–56. [CrossRef] [PubMed]

16. Tsai, W.-T.; Liu, S.-C.; Chen, H.-R.; Chang, Y.-M.; Tsai, Y.-L. Textural and chemical properties of swine-manure-derived biochar pertinent to its potential use as a soil amendment. *Chemosphere* **2012**, *89*, 198–203. [CrossRef] [PubMed]
17. Yao, Y.; Gao, B.; Inyang, M.; Zimmerman, A.; Cao, X.; Pullammanappallil, P.; Yang, L. Removal of phosphate from aqueous solution by biochar derived from anaerobically digested sugar beet tailings. *J. Hazard. Mater.* **2011**, *190*, 501–507. [CrossRef] [PubMed]
18. Gaskin, J.W.; Steiner, C.; Harris, K.; Das, K.C.; Bibens, B. Effect of Low-Temperature Pyrolysis Conditions on Biochar for Agricultural Use. *Trans. ASABE* **2008**, *51*, 2061–2069. [CrossRef]
19. Van Zwieten, L.; Kimber, S.; Morris, S.; Chan, K.Y.; Downie, A.; Rust, J.; Cowie, A. Effects of biochar from slow pyrolysis of papermill waste on agronomic performance and soil fertility. *Plant Soil* **2010**, *327*, 235–246. [CrossRef]
20. Doan, T.T.; Henry-Des-Tureaux, T.; Rumpel, C.; Janeau, J.-L.; Jouquet, P. Impact of compost, vermicompost and biochar on soil fertility, maize yield and soil erosion in Northern Vietnam: A three year mesocosm experiment. *Sci. Total Environ.* **2015**, *514*, 147–154. [CrossRef]
21. Ahmad, M.; Rajapaksha, A.U.; Lim, J.E.; Zhang, M.; Bolan, N.; Mohan, D.; Withanage, M.; Lee, S.S.; Ok, Y.S. Biochar as a sorbent for contaminant management in soil and water: A review. *Chemosphere* **2014**, *99*, 19–33. [CrossRef] [PubMed]
22. Zhao, L.; Cao, X.; Mašek, O.; Zimmerman, A. Heterogeneity of biochar properties as a function of feedstock sources and production temperatures. *J. Hazard. Mater.* **2013**, *256–257*, 1–9. [CrossRef]
23. Jefery, S.; Meinders, M.B.; Stoof, C.R.; Bezemer, T.M.; van de Voorde, T.F.J.; Mommer, L.; van Groenigen, J.W. Biochar application does not improve the soil hydrological function of a sandy soil. *Geoderma* **2015**, *251*, 47–54. [CrossRef]
24. Atkinson, C.J.; Fitzgerald, J.D.; Hipps, N.A. Potential mechanisms for achieving agricultural benefits from biochar application to temperate soils: A review. *Plant Soil* **2010**, *337*, 1–18. [CrossRef]
25. Tomczyk, A.; Sokołowska, Z.; Boguta, P. Biochar physicochemical properties: Pyrolysis temperature and feedstock kind effects. *Rev. Environ. Sci. Biotechnol.* **2020**, *19*, 191–215. [CrossRef]
26. Cantrell, K.B.; Hunt, P.G.; Uchimiya, M.; Novak, J.M.; Ro, K.S. Impact of pyrolysis temperature and manure source on physicochemical characteristics of biochar. *Bioresour. Technol.* **2012**, *107*, 419–428. [CrossRef]
27. Pariyar, P.; Kumari, K.; Jain, M.K.; Jadhao, P.S. Evaluation of change in biochar properties derived from different feedstock and pyrolysis temperature for environmental and agricultural application. *Sci. Total Environ.* **2020**, *713*, 136433. [CrossRef]
28. Manyà, J.J. Pyrolysis for Biochar Purposes: A Review to Establish Current Knowledge Gaps and Research Needs. *Environ. Sci. Technol.* **2012**, *46*, 7939–7954. [CrossRef]
29. Gaunt, J.L.; Lehmann, J. Energy balance and emissions associated with biochar sequestration and pyrolysis bioen-ergy production. *Environ. Sci. Technol.* **2008**, *42*, 4152–4158. [CrossRef]
30. Sohi, S.; Lopez-Capel, E.; Krull, E.; Bol, R. Biochar, climate change and soil: A review to guide future research. *CSIRO Land Water Sci. Rep.* **2009**, *5*, 17–31.
31. Antal, M.J.; Grønli, M.G. The Art, Science, and Technology of Charcoal Production. *Ind. Eng. Chem. Res.* **2003**, *42*, 1619–1640. [CrossRef]
32. Inguanzo, M.; Domínguez, A.; Menéndez, J.; Blanco, C.; Pis, J. On the pyrolysis of sewage sludge: The influence of pyrolysis conditions on solid, liquid and gas fractions. *J. Anal. Appl. Pyrolysis* **2002**, *63*, 209–222. [CrossRef]
33. Lu, H.; Zhang, W.; Wang, S.; Zhuang, L.; Yang, Y.; Qiu, R. Characterization of sewage sludge-derived biochars from different feedstocks and pyrolysis temperatures. *J. Anal. Appl. Pyrolysis* **2013**, *102*, 137–143. [CrossRef]
34. Park, J.; Lee, Y.; Ryu, C.; Park, Y.-K. Slow pyrolysis of rice straw: Analysis of products properties, carbon and energy yields. *Bioresour. Technol.* **2014**, *155*, 63–70. [CrossRef] [PubMed]
35. Schenkel, Y.; Bertaux, P.; Vanwijnbserghe, S.; Carre, J. An evaluation of the mound kiln carbonization technique. *Biomass Bioenergy* **1998**, *14*, 505–516. [CrossRef]
36. Shao, A.; Chen, H.; Yan, R.; Wang, X.; Yang, H.; Zhang, S. Study on Effect of Pyrolysis Temperature on Yield and Characteristics of Sludge Pyrolysis Semi-coke. *Renew. Energy* **2008**, *26*, 31–34.
37. Mackay, D.; Roberts, P. The influence of pyrolysis conditions on yield and microporosity of lignocellulosic chars. *Carbon* **1982**, *20*, 95–104. [CrossRef]
38. Dai, X.; Antal, M.J. Synthesis of a High-Yield Activated Carbon by Air Gasification of Macadamia Nut Shell Charcoal. *Ind. Eng. Chem. Res.* **1999**, *38*, 3386–3395. [CrossRef]
39. Culliney, T.W. Benefits of Classical Biological Control for Managing Invasive Plants. *Crit. Rev. Plant. Sci.* **2005**, *24*, 131–150. [CrossRef]
40. Witt, A. Impacts of invasive plants and their sustainable management in agro-ecosystems in Africa: A. review. *CABI Afr. NRB* **2010**, 1102–1109.
41. Lu, J.; Wu, J.; Fu, Z.; Zhu, L. Water Hyacinth in China: A Sustainability Science-Based Management Framework. *Environ. Manag.* **2007**, *40*, 823–830. [CrossRef]
42. Gao, L.; Li, B.; Jin, L. Can water hyacinth (Eichhornia crassipes) be controlled by reducing nitrogen and phosphorus pollution of water bodies? *Appl. Ecol. Environ. Res.* **2016**, *14*, 77–91. [CrossRef]
43. Lian, W.; Yang, L.; Joseph, S.; Shi, W.; Bian, R.; Zheng, J.; Li, L.; Shan, S.; Pan, G. Utilization of biochar produced from invasive plant species to efficiently adsorb Cd (II) and Pb (II). *Bioresour. Technol.* **2020**, *317*, 124011. [CrossRef]

44. Ahmed, M.B.; Zhou, J.L.; Ngo, H.H.; Guo, W. Insight into biochar properties and its cost analysis. *Biomass Bioenergy* **2016**, *84*, 76–86. [CrossRef]
45. Al-Wabel, M.I.; Hussain, Q.; Usman, A.R.; Ahmad, M.; Abduljabbar, A.; Sallam, A.S.; Ok, Y.S. Impact of biochar prop-erties on soil conditions and agricultural sustainability: A review. *Land Degrad. Dev.* **2018**, *29*, 2124–2161. [CrossRef]
46. Jiang, H.; Ye, Y.; Lu, P.; Zhao, M.; Xu, G.; Chen, D.; Song, T. Effects of torrefaction conditions on the hygroscopicity of biochars. *J. Energy Inst.* **2021**, *96*, 260–268. [CrossRef]
47. Dias, D.D.S.; Faria, F.A.; Mattiolli, L.; Capela, M.V.; Capela, J.M.V.; Crespi, M.S.; Ribeiro, C.A. Moisture sorption of biochar from banana pseudostem fibers according to the pyrolysis temperature. *J. Therm. Anal. Calorim.* **2019**, *138*, 3825–3832. [CrossRef]
48. Chen, H.; Lin, G.; Wang, X.; Chen, Y.; Liu, Y.; Yang, H. Physicochemical properties and hygroscopicity of tobacco stem biochar pyrolyzed at different temperatures. *J. Renew. Sustain. Energy* **2016**, *8*, 013112. [CrossRef]
49. Huang, H.; Reddy, N.G.; Huang, X.; Chen, P.; Wang, P.; Zhang, Y.; Garg, A. Effects of pyrolysis temperature, feedstock type and compaction on water retention of biochar amended soil. *Sci. Rep.* **2021**, *11*, 7419. [CrossRef] [PubMed]
50. Sohi, S.P.; Krull, E.; Lopez-Capel, E.; Bol, R. A review of biochar and its use and function in soil. In *Advances in Agronomy*; Elsevier: Amsterdam, The Netherlands, 2010; Volume 105, pp. 47–82.
51. Batista, E.M.C.C.; Shultz, J.; Matos, T.T.S.; Fornari, M.R.; Ferreira, T.M.; Szpoganicz, B.; de Freitas, R.; Mangrich, A.S. Effect of surface and porosity of biochar on water holding capacity aiming indirectly at preservation of the Amazon biome. *Sci. Rep.* **2018**, *8*, 10688. [CrossRef] [PubMed]
52. Kumar, H.; Cai, W.; Lai, J.; Chen, P.; Ganesan, S.P.; Bordoloi, S.; Liu, X.; Wen, Y.; Garg, A.; Mei, G. Influence of in-house produced biochars on cracks and retained water during drying-wetting cycles: Comparison between conventional plant, animal, and nano-biochars. *J. Soils Sediments* **2020**, *20*, 1983–1996. [CrossRef]
53. Bordoloi, S.; Kumar, H.; Hussain, R.; Karangat, R.; Lin, P.; Sreedeep, S.; Zhu, H.-H. Assessment of hydro-mechanical properties of biochar-amended soil sourced from two contrasting feedstock. *Biomass Convers. Biorefinery* **2020**, 1–16. [CrossRef]
54. Verheijen, F.; Jeffery, S.; Bastos, A.C.; Van der Velde, M.; Diafas, I. Biochar application to soils. A critical scientific re-view of effects on soil properties, processes, and functions. *EUR* **2010**, *24099*, 162.
55. Brewer, C.E.; Unger, R.; Schmidt-Rohr, K.; Brown, R.C. Criteria to select biochars for field studies based on biochar chemical properties. *Bioenergy Res.* **2011**, *4*, 312–323. [CrossRef]
56. Das, D.D.; Schnitzer, M.I.; Monreal, C.M.; Mayer, P. Chemical composition of acid–base fractions separated from biooil derived by fast pyrolysis of chicken manure. *Bioresour. Technol.* **2009**, *100*, 6524–6532. [CrossRef] [PubMed]
57. Colthup, N.B.; Daly, L.H.; Wiberley, S.E. *Introduction to Infrared and Raman Spectroscopy*; Elsevier BV: Amsterdam, The Netherlands, 1975.
58. Shinogi, Y.; Yoshida, H.; Koizumi, T.; Yamaoka, M.; Saito, T. Basic characteristics of low-temperature carbon products from waste sludge. *Adv. Environ. Res.* **2002**, *7*, 661–665. [CrossRef]
59. Zhang, H.; Voroney, R.; Price, G. Effects of temperature and processing conditions on biochar chemical properties and their influence on soil C and N transformations. *Soil Biol. Biochem.* **2015**, *83*, 19–28. [CrossRef]
60. Weiler, M.; Naef, F. An experimental tracer study of the role of macropores in infiltration in grassland soils. *Hydrol. Process.* **2003**, *17*, 477–493. [CrossRef]
61. Chia, C.H.; Downie, A.; Munroe, P. Characteristics of biochar: Physical and structural properties. In *Biochar for Environmental Management*; Routledge: London, UK, 2015; pp. 121–142.
62. Abe, I.; Iwasaki, S.; Iwata, Y.; Kominami, H.; Kera, Y. Relationship between Production Method and Adsorption Prop-erty of Char. *TANSO* **1998**, *185*, 277–284. [CrossRef]
63. Cao, X.; Harris, W. Properties of dairy-manure-derived biochar pertinent to its potential use in remediation. *Bioresour. Technol.* **2010**, *101*, 5222–5228. [CrossRef]
64. Cameron, R.W.; Blanuša, T.; Taylor, J.E.; Salisbury, A.; Halstead, A.J.; Henricot, B.; Thompson, K. The domestic garden—Its contribution to urban green infrastructure. *Urban For. Urban Green.* **2012**, *11*, 129–137. [CrossRef]
65. Yenisoy-Karakaş, S.; Aygün, A.; Güneş, M.; Tahtasakal, E. Physical and chemical characteristics of polymer-based spherical activated carbon and its ability to adsorb organics. *Carbon* **2004**, *42*, 477–484. [CrossRef]
66. Yue, Z.H.A.O.; Baowei, Z.H.A.O.; Hui, L.I.U.; Liujun, L.I.; Xin, Z.H.A.N.G. Effect of pyrolysis temperature on physicochemical properties and hygroscopicity of biochar. *Environ. Chem.* **2020**, *7*, 2005–2012.
67. Yang, W.; Shang, J.; Li, B.; Flury, M. Surface and colloid properties of biochar and implications for transport in porous media. *Crit. Rev. Environ. Sci. Technol.* **2020**, *50*, 2484–2522. [CrossRef]
68. Lin, J.; Tong, S. Preparation and properties of biochar. *Environ. Sci. Technol.* **2015**, *38*, 54–58.
69. Rao, X.; Fang, Z.; Wang, J.; Zhou, Z. Preparation, characterization and adsorption properties of peanut-shells-derived biochar. *Environ. Sci. Technol.* **2017**, *40*, 14–18.
70. Chang, X.; Hu, X.; Jiang, Y.; Sun, H.; Mu, Z. Biochar made from wheat straw: Preparation and characterization. *Environ. Sci. Technol.* **2017**, *40*, 24–29.
71. Gray, M.; Johnson, M.G.; Dragila, M.I.; Kleber, M. Water uptake in biochars: The roles of porosity and hydrophobicity. *Biomass Bioenergy* **2014**, *61*, 196–205. [CrossRef]
72. Li, H.; Tan, Z. Preparation of high water-retaining biochar and its mechanism of alleviating drought stress in the soil and plant system. *Biochar* **2021**, 1–12. [CrossRef]

73. Pitman, S.D.; Daniels, C.; Ely, M.E. Green infrastructure as life support: Urban nature and climate change. *Trans. R. Soc. South. Aust.* **2015**, *139*, 97–112. [CrossRef]
74. Nagase, A. Novel application and reused materials for extensive green roof substrates and drainage layers in Japan—Plant growth and moisture uptake implementation. *Ecol. Eng.* **2020**, *153*, 105898. [CrossRef]
75. Bollman, M.A.; DeSantis, G.E.; DuChanois, R.M.; Etten-Bohm, M.; Olszyk, D.M.; Lambrinos, J.G.; Mayer, P.M. A framework for optimizing hydrologic performance of green roof media. *Ecol. Eng.* **2019**, *140*, 105589. [CrossRef] [PubMed]
76. Graceson, A.; Hare, M.; Hall, N.; Monaghan, J. Use of inorganic substrates and composted green waste in growing media for green roofs. *Biosyst. Eng.* **2014**, *124*, 1–7. [CrossRef]